

Effects of the equation of state on the bulk properties of maximally rotating neutron stars

P. S. Koliogiannis* and Ch. C. Moustakidis†

Department of Theoretical Physics, Aristotle University of Thessaloniki, 54124 Thessaloniki, Greece

(Received 31 July 2019; revised manuscript received 13 November 2019; published 29 January 2020)

Neutron stars are among the densest known objects in the universe and an ideal laboratory for the strange physics of supercondensed matter. While the simultaneous measurements of mass and radius of nonrotating neutron stars may impose constraints on the properties of the dense nuclear matter, the observation and study of maximally rotating ones, close to the mass-shedding limit, may lead to significantly further constraints. Theoretical predictions allow neutron stars to rotate extremely fast (even more than 2000 Hz). However, until this moment, the fastest observed rotating pulsar has a frequency of 716 Hz, much lower compared to the theoretical predictions. There are many suggestions for the mechanism which lead to this situation. In any case, the theoretical study of uniformly rotating neutron stars, along with accurate measurements, may offer rich information concerning the high-density part of the equation of state. In addition, neutron stars through their evolution may provide us with a criterion to determine the final fate of a rotating compact star. Sensitivity of bulk neutron stars properties on the equation of state at the mass-shedding limit are the main subject of the present study.

DOI: [10.1103/PhysRevC.101.015805](https://doi.org/10.1103/PhysRevC.101.015805)**I. INTRODUCTION**

Neutron stars are considered extraordinary astronomical laboratories for the physics of nuclear matter because, from an astrophysical point of view, they are objects with the most fascinating constitution of energy and matter in the Universe [1–3]. To be more specific, the observation of mass, as well as the radius, of slowly rotating (or nonrotating) neutron stars may provide us with useful constraints on the equation of state (EoS) of nuclear matter. In addition, neutron stars, due to their compactness, may rotate very fast compared to other astrophysical objects [4]. Henceforth, measurements of specific properties (including mainly the mass and radius, frequency, moment of inertia, quadrupole moment, etc.) of maximally rotating neutron stars, close to the mass-shedding limit (hereafter maximally rotating corresponds to the configuration close or at the Keplerian frequency) may lead to robust constraints on the EoS as well as on the constitution of nuclear matter at high densities.

The determination of the maximum neutron star mass is a long-standing issue in astrophysics since it is directly related with the identification of black holes and the unknown behavior of the nuclear matter at high densities. Until this moment, the most massive neutron stars measurements (in solar masses, M_{\odot}) include (a) PSR J1614-2230 ($M = 1.97 \pm 0.04 M_{\odot}$) [5] (or from recent elaboration of the observation $M = 1.928 \pm 0.017 M_{\odot}$ [6] and $M = 1.908 \pm 0.016 M_{\odot}$ [7]), (b) PSR J0348+0432 ($M = 2.01 \pm 0.04 M_{\odot}$) [8], (c) PSR J0740+6620 ($M = 2.14^{+0.10}_{-0.09} M_{\odot}$) [9], and (d) PSR J2215+5135 ($M = 2.27^{+0.17}_{-0.15} M_{\odot}$) [10]. In addition,

there is a detailed study concerning the spin frequency of rotating neutron stars (for a review see Refs. [11]). The fastest rotating pulsar that has been found is the J1748-244ad with a spin frequency of 716 Hz [12]. However, the issue is still open: *Why we have not observed pulsars with higher values of frequency which are predicted from the majority of theoretical models?* Moreover, *what limits the spin frequencies of millisecond pulsars and why?* [13]. Future measurements of moment of inertia [14] and Keplerian frequency may be the answer to these questions by improving considerably our knowledge on the properties of maximally rotating neutron stars.

The effects of the EoS on the properties of rotating neutron stars (see Refs. [15,16] for an introduction and relevant bibliography) had begun to gain ground in the late 1980s with Shapiro and Teukolsky and their colleagues [17–21]. A significant contribution on these issues had been also made from Friedman and his colleagues [22–26], Haensel and coworkers [27–32], as well as Glendenning and his colleagues [33–36]. Rapid rotation and its effects on the EoS had been studied also in Refs. [37–42] and most recently in Refs. [43–58]. Moreover, in nuclear astrophysics hot neutron stars in correlation with rapid rotation had been studied in Refs. [59,60]. In addition, maximally rotating neutron stars in modified gravity theories have been studied in detail by Kokkotas and his colleagues [61,62].

In this work we extend the previous fundamental work of Cook, Shapiro, and Teukolsky [20], as well as the most recent work of Cipolletta *et al.* [52]. In particular, we employ a large number of modern EoSs (combined with a few previous ones) which all of them, at least marginally (few of them), predict the upper bound of the maximum neutron star mass of $M = 1.908 \pm 0.016 M_{\odot}$ [7], while also reproducing accurately the bulk properties of symmetric nuclear

*pkoliogi@physics.auth.gr

†moustaki@auth.gr

matter (for more details see Ref. [63]). The models of these EoSs are phenomenological, field theoretical, and microscopic. In the category of phenomenological models, there are the momentum-dependent interaction model (MDI) [64,65], Heiselberg-Hjorth Jensen model (HHJ) [66], Skyrme model type a and type I4 (Ska, SkI4) [67,68], Douchin-Haensel model (DH) [69]; in field-theoretical category, there are the non-linear derivative model (NLD) [70,71], and Walecka model (W) [72]; and in the microscopic category, there are the Hebeler-Lattimer-Pethick-Schwenk model (HLPS) (based on nuclear interactions derived from chiral effective field theory) [73], Sharma-Centelles-Vinas-Baldo-Burgio model (SCVBB) (using the Argonne v18 potential plus three-body forces computed with the Urbana model) [74], Balberg-Shapiro model (BS) [75], Bowers-Gleeson-Pedigo model (BGP) (relativistic pion exchange) [76], Bombaci-Logoteta model (BL) [77], Wiringa-Fiks-Fabrocini model (WFF1, WFF2) [78], and Pandharipande-Smit model (PS) [79]. It has to be stressed that the majority of the mentioned EoSs have been constructed in order to reproduce the bulk properties of uniform symmetric nuclear matter and also to extend to pure neutron matter. The extension to neutron star matter is performed with respect to β equilibrium. As far as concerns the leptonic degree of freedom, in most of them it is considered that the main contribution of leptons is due to electrons. All of the used EoSs properly describe the fluid core of a neutron star. It should be noted also that few of them have been applied first for the study of finite nuclei. Among the number of equations that we use, we have constructed two EoSs, the Akmal-Pandharipande-Ravenhall model (APR-1, APR-2) (Microscopic model) [80], predicted by the MDI model. This model reproduces the results of microscopic calculations of symmetric nuclear matter and neutron star matter at zero temperature with the advantage of its extension to finite temperature. For the solid crust region of all the EoSs we employed the EoS of Feynman, Metropolis, and Teller [81] and also of Baym, Bethe, and Sutherland [82].

An effort was made to systematically study most of the bulk properties of uniformly rotating neutron stars at the Keplerian sequence (the sequence in which the maximum mass configuration corresponds to the Keplerian frequency), including the mass, polar and equatorial radius; angular velocity; moment of inertia; Kerr parameter; eccentricity; braking index; and so on. Additionally, for reasons of completeness and comparison, because all EoSs that we use are hadronic ones, we present also an EoS with appearance of hyperons at high densities (Florida State University model, FSU2H) [83] and one suitable to describe quark stars based on MIT bag model (quark star model, QS57.6) [2,3].

Furthermore, we explore the possibility to update the previous empirical universal relations which connect the Keplerian frequency with the mass and radius at the maximum mass configuration. We systematically study the Kerr parameter dependence on the EoS and also provide the evolution of the angular momentum of a neutron star in order to examine the case where neutron stars considered to be progenitors of black holes. In particular, we examine (according to the terminology of Ref. [20]) two equilibrium sequences of rotating neutron stars, *normal* and *supramassive*. While *normal* evolutionary

sequences have a spherical, nonrotating (stable) end point, *supramassive* ones, which by definition have masses higher than the maximum mass of the nonrotating neutron star, they do not have a stable end point and, as a consequence, the collapse to a black hole is inevitable. However, the construction of *normal* and mainly *supramassive* sequences is a complicated procedure in the framework of general relativity (GR) [20].

In addition, we systematically study the moment of inertia, a quantity which plays an important role in the properties of rotating neutron stars, and eccentricity, which can inform us about their deformation. Following the previous work of Lattimer and Prakash [84], we also provide an absolute upper limit of the higher density of cold baryonic matter in the Universe, based on the upper limit imposed by the maximum mass of a neutron star. In fact, we try to improve the bound which was introduced in Ref. [84] by using updated EoSs and including also the case of maximally rotating neutron stars. Finally, we study the effects of the EoS on the braking index of pulsars. We mainly focus on values near the Keplerian frequency (70% and more) where the braking index begins to be affected by the rest mass (definition has been given in a proper section).

The article is organized as follows. In Sec. II we briefly review the properties of nuclear matter, the computational hypothesis and the models for the nuclear EoSs. In Sec. III we present the rotating configuration for neutron stars. In particular, we introduce the effects of the Keplerian frequency on the bulk properties of neutron stars and we also describe two properties of the EoS, moment of inertia and eccentricity. In addition, we provide a discussion for the Kerr parameter and the fully described rest mass sequences. The upper bound for density of cold baryonic matter and the effects of the braking index on the EoS are also obtained. Section IV contains the discussion and main conclusions of the present study. Finally, useful expressions and clarifications are given in the Appendix.

II. THE NUCLEAR EQUATION OF STATE

In the present study we have suitably selected and employed a large number of hadronic EoSs [63]. Moreover, we have constructed two additional EoSs, the APR-1 and APR-2, by using the MDI model (for more details see Appendix A) and data from Akmal *et al.* [80]. Except the hadronic EoSs, an EoS with appearance of hyperons at high densities and one suitable to describe quark stars have been used for completeness [2,3,83].

There are many reasons to support the reliability of the MDI model. In particular, (a) it reproduces with high accuracy the properties of symmetric nuclear matter at the saturation density, (b) the theoretical prediction of the value and slope of symmetry energy at the saturation density are close to the experimental predictions, (c) it reproduces other properties of symmetric nuclear matter (SNM) (including isovector quantities K_0 and Q_0) inside the limiting area of the experimental data, (d) it reproduces correctly the microscopic calculation of the Chiral model [85] for pure neutron matter (PNM) (for low densities) and the results of *state-of-the-art* calculations

of Akmal *et al.* [80] (for high densities), (e) it has the flexibility that the energy per particle depends not only on the density but also on the momentum, (f) it can be easily extended to include temperature dependence (which is needed to study core-collapse supernova, protoneutron stars, neutron stars merger, etc.), and (g) it predicts a maximum neutron star mass that is higher than the observed ones [5–10].

A. Properties of nuclear matter and the construction of the APR-1 and APR-2 EoSs

Assuming that the neutron-proton asymmetry is characterized by the parameter [86,87]

$$I = \frac{n_n - n_p}{n} = 1 - 2x, \quad (1)$$

where n_p , n_n and $n = n_p + n_n$ are the proton, neutron, and total densities and $x = n_p/n$ is the proton fraction, the total energy per particle can be expanded as follows:

$$E(n, I) = E(n, 0) + \sum_{k=2,4,\dots} E_{\text{sym},k}(n)I^k, \quad (2)$$

where

$$E_{\text{sym},k}(n) = \frac{1}{k!} \left. \frac{\partial^k E(n, I)}{\partial I^k} \right|_{I=0}. \quad (3)$$

We studied two cases in this paper, the parabolic (symbolized as *pa*) and the full (symbolized as *f*) approximations. In the case of the parabolic approximation we considered that the symmetry energy is given through

$$E_{\text{sym},pa}(n) = E(n, I = 1) - E(n, I = 0), \quad (4)$$

while in the full approximation it is given through

$$E_{\text{sym},f}(n) = E_{\text{sym},2}(n) = S_2(n). \quad (5)$$

The properties of nuclear matter at the saturation density are defined as [86,87]

$$L = 3n_s \left. \frac{dS_2(n)}{dn} \right|_{n_s}, \quad K = 9n_s^2 \left. \frac{d^2S_2(n)}{dn^2} \right|_{n_s}, \quad (6)$$

$$Q = 27n_s^3 \left. \frac{d^3S_2(n)}{dn^3} \right|_{n_s}, \quad K_0 = 9n_s^2 \left. \frac{d^2E(n, 0)}{dn^2} \right|_{n_s}, \quad (7)$$

$$Q_0 = 27n_s^3 \left. \frac{d^3E(n, 0)}{dn^3} \right|_{n_s}, \quad (8)$$

where L , K , Q are related to the first, second, and third derivatives of the symmetry energy $S_2(n)$, respectively. K_0 is the compression modulus and Q_0 is related to the third derivative of $E(n, 0)$. The n_s is the saturation density of symmetric nuclear matter and its equal to 0.16 fm^{-3} . The last property is the ratio of the Landau effective mass to mass in

TABLE I. Properties of nuclear matter (NM) for APR-1 and APR-2 EoSs.

Properties of NM	APR-1	APR-2
L_{pa} (MeV)	63.18	57.43
Q_{pa} (MeV)	482.34	568.91
K_{pa} (MeV)	-103.70	-118.78
$E_{\text{sym},pa}$ (MeV)	33.61	33.59
L_f (MeV)	63.31	57.40
Q_f (MeV)	450.50	538.44
K_f (MeV)	-88.26	-99.81
$E_{\text{sym},f}$ (MeV)	32.74	32.53
Q_0 (MeV)	-581.27	-581.27
K_0 (MeV)	256.40	256.40
m_τ^*/m_τ	0.72	0.72

vacuum for the MDI model [64,86–89] and given by

$$\frac{m_\tau^*(n, I)}{m_\tau} = \left(1 - \frac{2nm_\tau}{n_s \hbar^2} \sum_{i=1,2} \frac{1}{\Lambda_i^2} \frac{C_i \pm \frac{C_i - 8Z_i I}{5}}{\left\{ 1 + \left(\frac{k_F^0}{\Lambda_i} \right)^2 \left[(1 \pm I) \frac{n}{n_s} \right]^{2/3} \right\}^2} \right)^{-1}, \quad (9)$$

where τ corresponds to neutrons or protons.

Although we studied two cases, the parabolic and full approximation, the one that is used in the detailed study is the full approximation. Both of them lead to similar results. However, the parabolic approximation is referenced for future studies.

The parametrization of the MDI model [Eq. (A1)] is performed by using data originated from the work of Akmal *et al.* [80]. In particular, we employed the data concerning the energy per particle of symmetric and pure neutron matter (in the area $0.04 \text{ fm}^{-3} \leq n \leq 0.96 \text{ fm}^{-3}$) and for models A18 + UIX (hereafter APR-1) and A18 + δv + UIX* (hereafter APR-2). In order to achieve the best fitting to Akmal's data using Eq. (A1), we divided our region of study into three sections: (a) low-density region ($0.04 \text{ fm}^{-3} \leq n \leq 0.2 \text{ fm}^{-3}$), (b) medium-density region ($0.2 \text{ fm}^{-3} \leq n \leq 0.56 \text{ fm}^{-3}$), and (c) high-density region ($0.56 \text{ fm}^{-3} \leq n \leq 0.96 \text{ fm}^{-3}$). With this method we have calculated the coupling constants and the parameters for the asymmetric nuclear matter.

The main properties of nuclear matter at the saturation density n_s , calculated with Eq. (4) through Eq. (9) for the APR-1 and APR-2 EoSs, including also isovector quantities, are presented in Table I. It should be noted that the parametrization of pure neutron matter leads to results in agreement with the predictions of chiral effective field theory [85] for low densities. For high-density values, the parametrization leads to the prediction of Akmal *et al.* [80]. The main drawback of these two EoSs is related with the violation of causality; the speed of sound becomes greater than the speed of light at high densities. However, the parametrization of the MDI model has the advantage that prevents the onset from violating the causality.

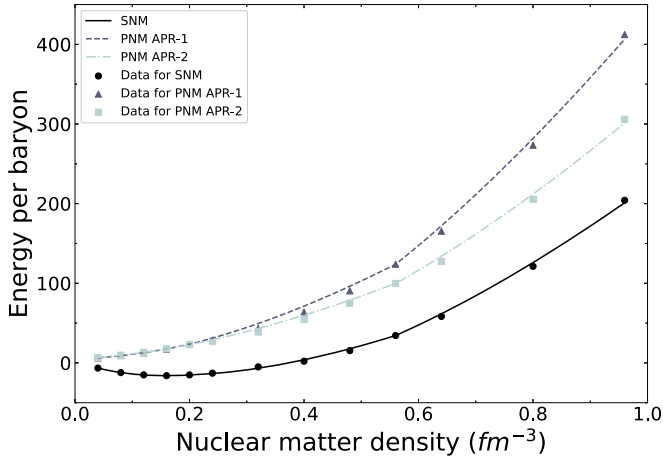


FIG. 1. Symmetric nuclear matter and pure neutron matter fits for APR EoSs using Akmal’s [80] data and the MDI model. The SNM is presented with the circles and the solid line, the APR-1 PNM is presented with the triangles and the dashed line, and the APR-2 PNM is presented with the squares and the dashed-dotted line.

The schematic presentation of Eq. (A1) for APR EoSs and the data from Akmal *et al.* [80] are presented in Fig. 1.

B. The selected equations of state

The EoSs that we used [63–80] are consistent with the current observed limits of neutron star mass [5–10] and also with the one for frequency [12]. In Fig. 2 we present the gravitational mass versus the corresponding equatorial radius (hereafter radius) for the 23 EoSs at the nonrotating configuration, where the current observed limits are also presented.

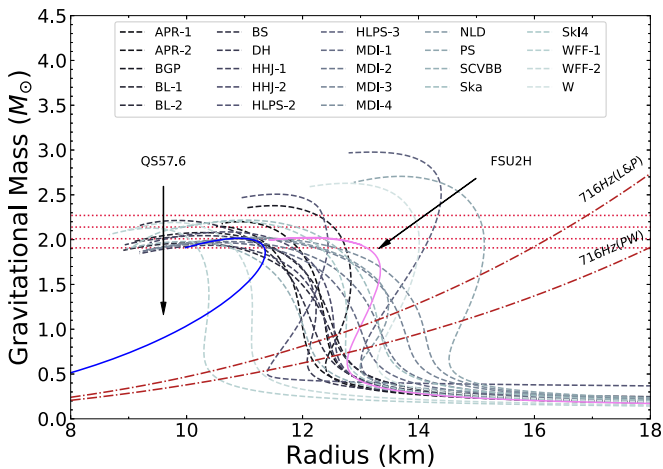


FIG. 2. Mass-radius diagram for the 23 EoSs at the nonrotating configuration. The observed limits of neutron star mass are presented with the horizontal dotted lines ($1.908M_{\odot}$, $2.01M_{\odot}$, $2.14M_{\odot}$, and $2.27M_{\odot}$). The observed limit of 716 Hz, from Lattimer and Prakash (L&P) [90] and from the present work (PW) (for more details see Appendix B), is presented with the curved dashed-dotted lines. The two indicated solid lines correspond to the EoS with appearance of hyperons at high densities (FSU2H) and the one suitable to describe quark stars (QS57.6).

Moreover, the EoS with appearance of hyperons at high densities (FSU2H) and the one suitable to describe quark stars (QS57.6) are also indicated.

III. ROTATING NEUTRON STARS

In the framework of general relativity rotating neutron stars can be described (a) by the stationary axisymmetric space-time metric [4,16]

$$ds^2 = -e^{2\nu} dt^2 + e^{2\psi} (d\phi - \omega dt)^2 + e^{2\mu} (dr^2 + r^2 d\theta^2), \quad (10)$$

where the metric functions ν , ψ , ω , and μ depend only on the coordinates r and θ and (b) the matter inside the neutron star. If we neglect sources of nonisotropic stresses, as well as viscous ones and heat transport, then the matter inside the neutron star can be fully described by the stress-energy tensor and modeled as a perfect fluid [4,16],

$$T^{\alpha\beta} = (\varepsilon + P)u^{\alpha}u^{\beta} + Pg^{\alpha\beta}, \quad (11)$$

where u^{α} is the fluid’s four-velocity. The energy density and pressure is denoted as ε and P .

For the numerical integration of the equilibrium equations we used the public RNS code [91] by Stergioulas and Friedman [92] (this code is based on the method developed by Komatsu, Eriguchi, and Hachisu [93] and modifications introduced by Cook, Shapiro and Teukolsky [19]).

A. Keplerian frequency

The derivation of the Keplerian frequency, in which a rotating star would shed matter at its equator, is a complicated problem. In Newtonian theory, it has its origin on the balance between gravitational and centrifugal forces and takes a very simple form. However, in GR it exhibits a more complicated dependence on the structure of the star through the interior metric as it is expressed as a self-consistency condition that must be satisfied by the solution to Einstein’s equations.

It has been shown by Friedman *et al.* [24] that the turning-point method, which leads to the points of secular instability, can also be used in the case of uniformly rotating neutron stars. With this consideration, in a constant angular momentum sequence, the turning-point of a sequence of configurations with increasing central density separates the secular stable from unstable configuration and, consequently, the condition

$$\left. \frac{\partial M(\varepsilon_c, J)}{\partial \varepsilon_c} \right|_{J=\text{constant}} = 0, \quad (12)$$

where ε_c is the energy density in the center of the neutron star and J is the angular momentum, defines the possible maximum gravitational mass. In general, gravitational (gr) and rest mass (rm) are defined as [3]

$$M_{\text{gr}} = \int_0^R 4\pi r^2 \varepsilon(r) dr, \quad (13)$$

$$M_{\text{rm}} = m_A \int_0^R 4\pi r^2 \frac{n(r)}{\left[1 - \frac{2GM(r)}{c^2 r}\right]^{1/2}} dr, \quad (14)$$

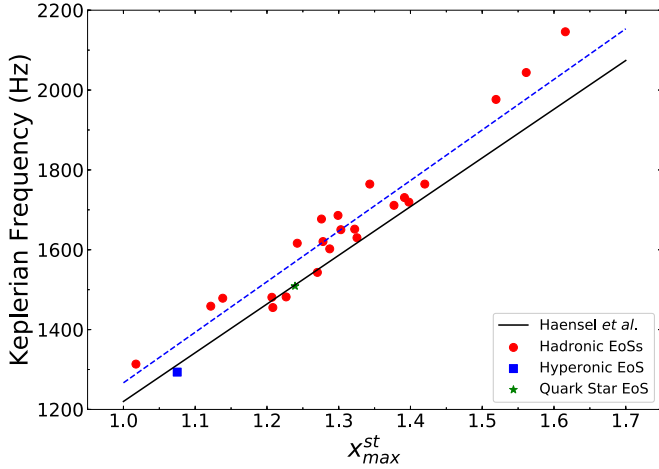


FIG. 3. Keplerian frequency dependence on the quantity x_{\max}^{st} for the 23 EoSs [for more details see Eq. (16)]. Blue dashed line corresponds to the best linear trend that fits the data. The data from 23 hadronic EoSs are also presented with red circles. The hyperonic EoS is indicated with the blue square and the quark star EoS with the green star. The black solid line marks the work of Haensel *et al.* [48].

where m_A is the baryonic mass and $n(r)$ is the baryon number density.

The absence of analytical solutions for rotating neutron stars leads to numerical estimations for the Keplerian frequency. A significant number of empirical formulas for the Keplerian frequency had been produced along the years. The formula is given by [48,57]

$$f_k = C_\alpha \left(\frac{M_{\max}^\alpha}{M_\odot} \right)^{1/2} \left(\frac{10 \text{ km}}{R_{\max}^\alpha} \right)^{3/2} = C_\alpha x_{\max}^\alpha \text{ (Hz)}, \quad (15)$$

where

$$x_{\max}^\alpha = \left(\frac{M_{\max}^\alpha}{M_\odot} \right)^{1/2} \left(\frac{10 \text{ km}}{R_{\max}^\alpha} \right)^{3/2} \quad (16)$$

and α (st : static, rot : rotating, rm;rot : rest mass at rotating configuration) takes the form of the corresponding configuration. Although this relation is well established, the unknown parameter (C_α) depends highly on the various approximations and of course the selected EoSs.

It is worth pointing out that while the maximum rotation rate is an increasing function of the EoS's softness, the maximum mass is a decreasing one (considering a fixed mass). Therefore, for a fixed gravitational mass M the softer EoS predicts the lower value of the radius R and, consequently, leads to higher values for f_k . The latter had been already noticed by Lattimer *et al.* [39]. These two constraints restrict the EoS in a narrow region. The above statement is one of the main subjects of the present work.

1. The Keplerian frequency, the maximum mass, and the corresponding radius of nonrotating neutron stars

We studied the Keplerian frequency in correlation with the bulk properties of a nonrotating neutron star and specifically on its gravitational mass and the corresponding radius at the maximum mass configuration, using Eq. (15) and $\alpha = \text{st}$.

TABLE II. Parametrization of Eq. (15) for the different configurations. The relative error (r.e.) between the data and fits is also presented.

α	C_α	r.e.%	C_{Haensel}
st	1266.68	5.6	1220
rot	1781.90	≤ 1	—
rm;rot	1644.75	2.2	—

In Fig. 3 we present the relation (15) with the corresponding parametrization, which can be found in Table II, updating the work of Haensel *et al.* [48]. The value of the parameter C_{st} is in very good agreement with the current EoSs to a linear term.

2. The Keplerian frequency, the maximum mass, and the corresponding radius of maximally rotating neutron stars

An interesting relation is also the one between the Keplerian frequency and the macroscopic properties of maximally rotating neutron stars (maximum gravitational mass and the corresponding radius). Using Eq. (15) and $\alpha = \text{rot}$, it is remarkable that in this scenario, as Fig. 4(a) shows, the linear fit between these quantities ($f_k, x_{\max}^{\text{rot}}$) leads to nearly perfect results. The parametrization can be found in Table II.

3. The Keplerian frequency, the maximum rest mass, and the corresponding radius of maximally rotating neutron stars

In the macroscopic properties of a neutron star, rest mass plays an important role. In order to understand the effects of the rest mass on the Keplerian sequence, we studied the Keplerian frequency dependence on the rest mass and the corresponding radius using Eq. (15) and $\alpha = \text{rm;rot}$.

In Fig. 4(b) we can see the almost linear relation that holds between these two quantities ($f_k, x_{\max}^{\text{rm;rot}}$), enhancing the existence of a relation between rest mass and gravitational mass in neutron stars at the Keplerian frequency. The parametrization can be found in Table II.

4. Rest mass and gravitational mass at the maximum mass configuration of maximally rotating neutron stars

As a follow-up to Sec. III A 3, we studied the rest mass dependence on the gravitational mass at the maximum mass configuration for the Keplerian frequency. In Fig. 5, we can see the almost linear relation between these two quantities, as expected from Sec. III A 3.

The relation which describes our data is given via the form

$$\left(\frac{M_{\max}^{\text{rm;rot}}}{M_\odot} \right) = 1.17 \left(\frac{M_{\max}^{\text{gm;rot}}}{M_\odot} \right) \quad (17)$$

(the maximum possible error is less than 3.3%), concluding that the percentage difference between these quantities is around 17%.

B. Moment of inertia and eccentricity

Rotating neutron stars can provide us with more quantities than nonrotating ones that we could study. Among them, there

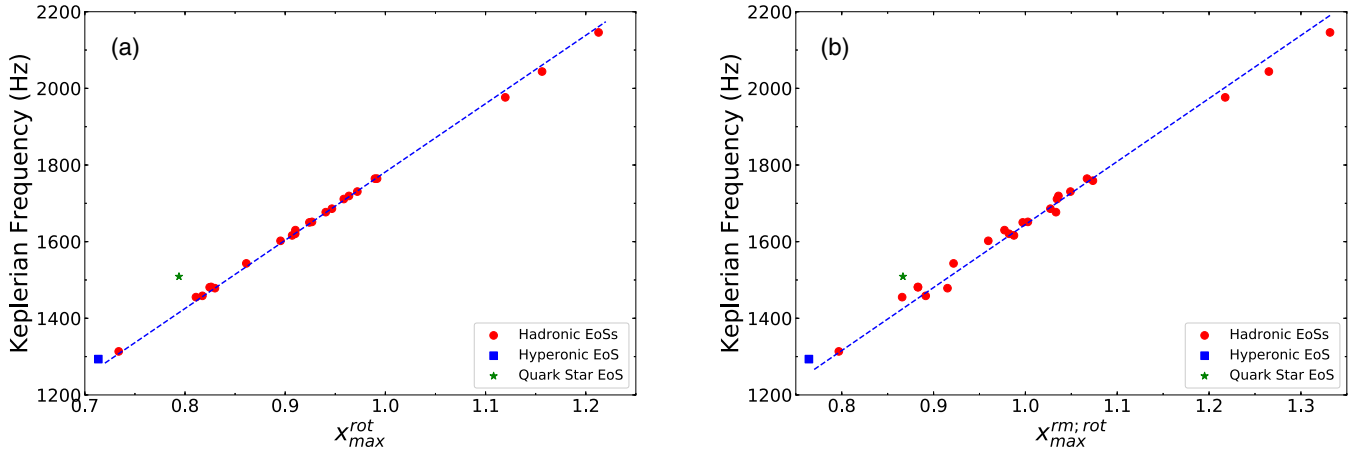


FIG. 4. Keplerian frequency dependence on the quantity (a) x_{\max}^{rot} and (b) $x_{\max}^{\text{rm:rot}}$ for the 23 EoSs [for more details see Eq. (16)]. Blue dashed lines correspond to the best linear trend that fits the data. The data from 23 hadronic EoSs are also presented with red circles. The hyperonic EoS is indicated with the blue square and the quark star EoS with the green star.

is the moment of inertia and eccentricity. Both these quantities can give us information about the deformation of the mass while its spinning.

The moment of inertia [52,94], which have a prominent role in pulsar analysis, is defined as

$$I = \frac{J}{\Omega}, \quad (18)$$

where J is the angular momentum and Ω is the angular velocity. This property of neutron stars quantifies how fast an object can spin with a given angular momentum.

We studied the moment of inertia dependence on the gravitational mass for the Keplerian sequence. From Fig. 6(a) we can see that all EoSs present similar behavior. For this reason, inside Fig. 6(a), we plotted the moment of inertia values corresponding to maximum mass configuration versus

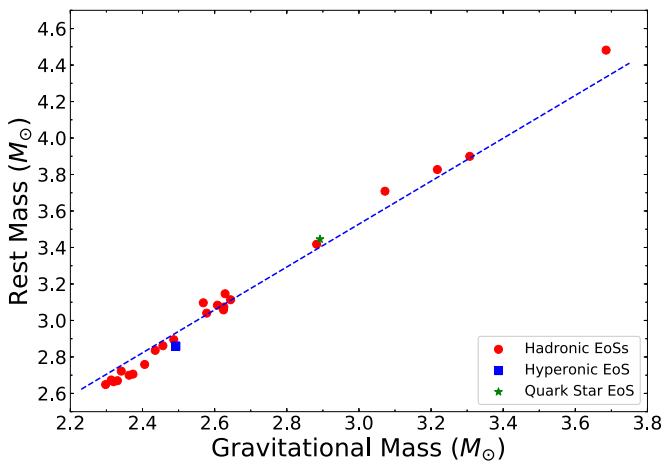


FIG. 5. Rest mass dependence on the gravitational mass of a maximally rotating neutron star at the maximum mass configuration. Blue dashed line corresponds to the best linear trend that fits the data. The data from 23 hadronic EoSs are also presented with red circles. The hyperonic EoS is indicated with the blue square and the quark star EoS with the green star.

the corresponding gravitational mass. A relation, given by the formula

$$I_{\max}^{\text{rot}} = -1.568 + 0.883 \exp \left[0.7 \left(\frac{M_{\max}^{\text{gm:rot}}}{M_{\odot}} \right) \right] (10^{45} \text{ gr cm}^2), \quad (19)$$

describes with high accuracy our data, concluding that moment of inertia, at the maximum mass configuration for the Keplerian frequency, can provide us with a universal relation between moment of inertia and the corresponding gravitational mass.

We also studied the dimensionless moment of inertia dependence on the corresponding compactness parameter [95], which, in general, it is defined as

$$\beta = \frac{GM}{Rc^2}, \quad (20)$$

where R corresponds to the equatorial radius of neutron star.

In Fig. 6(b) we present a window where moment of inertia and compactness parameter can lie [shaded (gray) region], constraining both these quantities. There is an empirical relation, derived from the data, that can describe this window. The form of this empirical relation is

$$I/MR^2 = \alpha_1 + \alpha_2\beta + \alpha_3\beta^2 + \alpha_4\beta^3 + \alpha_5\beta^4, \quad (21)$$

where the coefficients for the two edges are shown in Table III. It is clear from Fig. 6(b) and Eq. (21) that if we have a measurement of moment of inertia, or compactness parameter, then we could extract the interval where the other parameter can lie.

As a consequence, by constraining simultaneously these two quantities, we could impose constraints on the radius of neutron stars, which still remains an open problem.

From Fig. 6(b) we can see that all EoSs present similar behavior. For this reason, inside Fig. 6(b), we plotted the dimensionless moment of inertia values corresponding to maximum mass configuration versus the corresponding compactness parameter. A relation, given by the formula

$$(I/MR^2)_{\max} = -0.006 + 1.379\beta_{\max}, \quad (22)$$

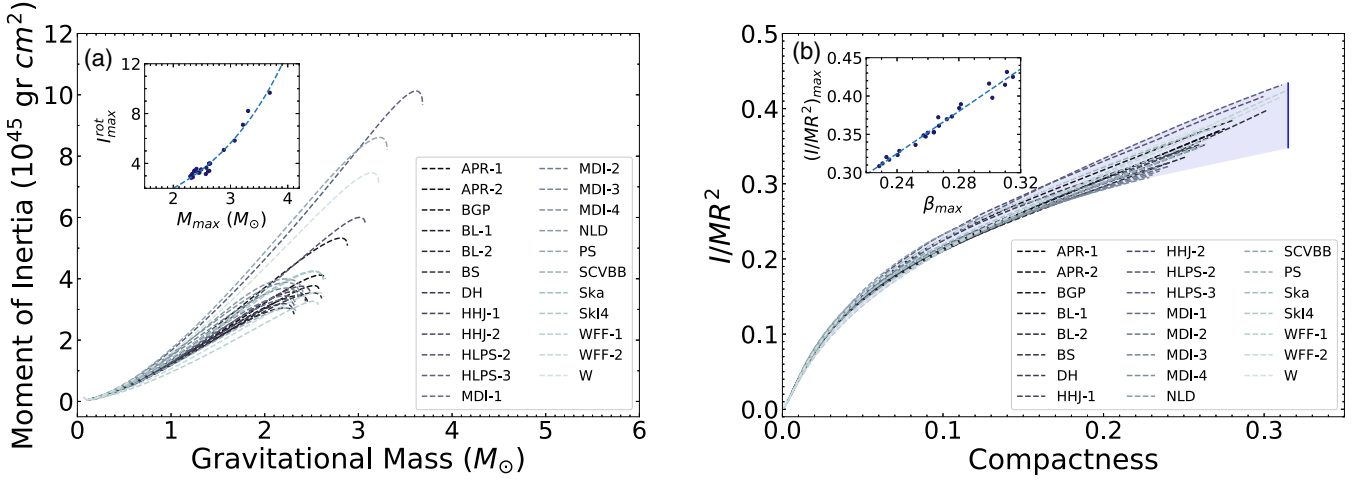


FIG. 6. Moment of inertia dependence (a) on the gravitational mass and (b) on the compactness parameter of a maximally rotating neutron star for the 23 EoSs. Blue dashed lines in the inside figures correspond to the best fit in each case. The data at the maximum mass configuration are also presented with blue circles in the inside figures.

describes with high accuracy our data, concluding that dimensionless moment of inertia, at the maximum mass configuration for the Keplerian frequency, can provide us with a universal relation between dimensionless moment of inertia and the corresponding compactness parameter.

Eccentricity is the main quantity that is related to the deformation of the star. Rapid rotation deforms the models of equilibrium and in order to see how these models change we calculate the eccentricity, which is given by the form [52]

$$\epsilon = \sqrt{1 - \left(\frac{r_{\text{pol}}}{r_{\text{eq}}}\right)^2}, \quad (23)$$

where the r_{pol} and r_{eq} are the polar and equatorial radius of the star, respectively.

For a schematic presentation of the energy inside a neutron star, in Fig. 7 we present the contours of constant density of a neutron star model with central density equals to $10^{15} \text{ gr cm}^{-3}$, both in the nonrotating case and in the rotating one with frequency equals to the Keplerian frequency. For the sake of example we used the APR-1 EoS.

Performing the same analysis as for moment of inertia, we studied the eccentricity dependence on the gravitational mass for the Keplerian sequence and the eccentricity values corresponding to maximum mass configuration on the corresponding gravitational mass, as Fig. 8 shows. A relation, given by the formula

$$\epsilon_{\text{max}} = 0.799 + 0.01 \left(\frac{M_{\text{max}}}{M_{\odot}}\right), \quad (24)$$

TABLE III. Coefficients of the empirical relation (21) for the two edges of the window presented in Fig. 6(b).

Edges	α_1	α_2	α_3	α_4	α_5
Upper	0.005	4.01	-24.79	86.66	-110.33
Lower	0.005	3.38	-17.45	49.68	-55.36

describes with high accuracy our data, concluding that eccentricity, at the maximum mass configuration for the Keplerian frequency, is an EoS-independent property.

C. The Kerr parameter

The Kerr space-time provided from Einstein's field equations give us the so-called Kerr black holes [49,52]. These rotating black holes can be fully described from the gravitational mass (M) and the angular momentum (J). In order to have a meaningful Kerr black hole, the relation $J \geq GM^2/c$ (Kerr bound) must hold, or otherwise, we have a naked singularity. A naked singularity is a black hole without a horizon and can be considered as closed timelike curves, where causality would be violated. While there is no rigorous proof from Einstein's field equations, the cosmic-censorship conjecture implies that a generic gravitational collapse cannot form a naked singularity [96–99]. This is why the astrophysical black holes should satisfy the Kerr bound [49,52].

The gravitational collapse of a massive rotating neutron star, constrained to mass-energy and angular momentum conservation, creates a black hole with almost the same mass and angular momentum as the prior neutron star. In this case, an important quantity to study, directly related with black holes as well as neutron stars, is the dimensionless angular momentum [51], which is defined as

$$j = \frac{cJ}{GM_{\odot}^2} \quad (25)$$

and it is known as dimensionless spin parameter. As a consequence of this parameter, we can define a new one, starting from the parameter α , which is the angular momentum in units of mass and it is given by the form [16]

$$\alpha \equiv \frac{J}{M} = j \frac{GM_{\odot}^2}{c} \frac{1}{M}. \quad (26)$$

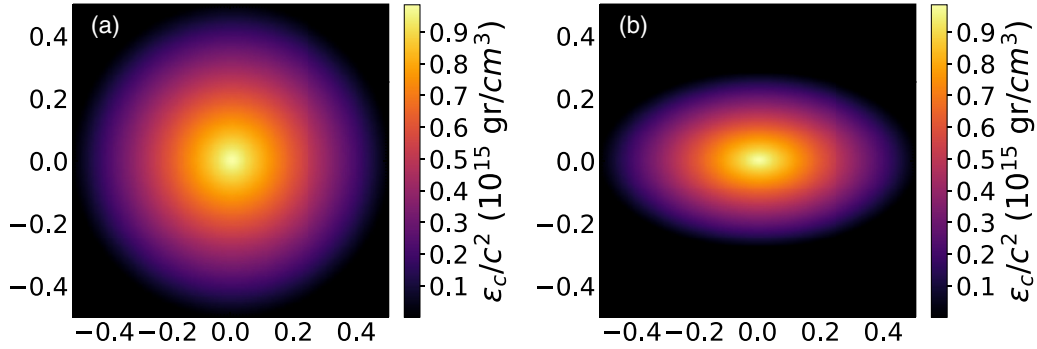


FIG. 7. Contours of constant density of a neutron star model with central density equals 10^{15} gr/cm^3 both (a) in the nonrotating case and (b) in the rotating one with frequency equals to the Keplerian frequency for the APR-1 EoS. The axis had been scaled in a way that the maximum radius corresponds to 0.5.

Next, using Eq. (26), the well-known *Kerr parameter* takes the form

$$\mathcal{K} = \frac{\alpha}{M} \frac{c}{G} = j \left(\frac{M_{\odot}}{M} \right)^2. \quad (27)$$

The dependence of this parameter on the gravitational mass at the Keplerian sequence can be seen in Fig. 9.

Although the meaning of this parameter at black-holes physics is so interesting and fundamental (there is a maximum value at 0.998 [100]), that is also the case for other compact objects such as neutron stars. In order to find a way to constrain the value of the Kerr parameter in neutron stars, we studied the dependence of this parameter on the total gravitational mass for the Keplerian sequence. From Fig. 9, we can see that the maximum value of the Kerr parameter for neutron stars is around 0.75. While there is a number of EoSs that hold on near this value, the maximum value achieved from HLPS-3. This EoS is the stiffest equation that we have and produces maximum mass greater than all the others. Strictly speaking, if we consider this EoS as the one

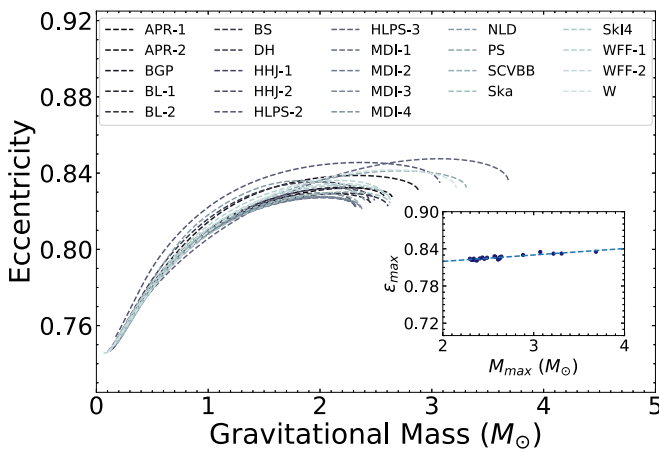


FIG. 8. Eccentricity dependence on the gravitational mass of a maximally rotating neutron star. Inset: The eccentricity values as a function of the corresponding gravitational mass at the maximum mass configuration. Blue dashed line in the inside figure corresponds to the best fit. The data at the maximum mass configuration are also presented with blue circles in the inside figure.

that produces the maximum possible mass in the maximum mass configuration at the Keplerian sequence, then we could constrain the maximum value of the Kerr parameter in neutron stars.

In Fig. 9 we present also a window [shadowed (gray) region] where the Kerr parameter can lie. There is an empirical relation, derived from the data, that can describe this window. The form of this empirical relation is

$$\mathcal{K} = d_1 + d_2 \coth \left[d_3 \left(\frac{M_{\max}}{M_{\odot}} \right) \right], \quad (28)$$

where the coefficients for the two edges are shown in Table IV. It is clear from Fig. 9 and Eq. (28) that if we have a measurement of gravitational mass, or spin parameter, then we could extract the interval where the other parameter can lie.

As a consequence, by measuring accurately and simultaneously these two quantities, we could impose constraints on the EoS.

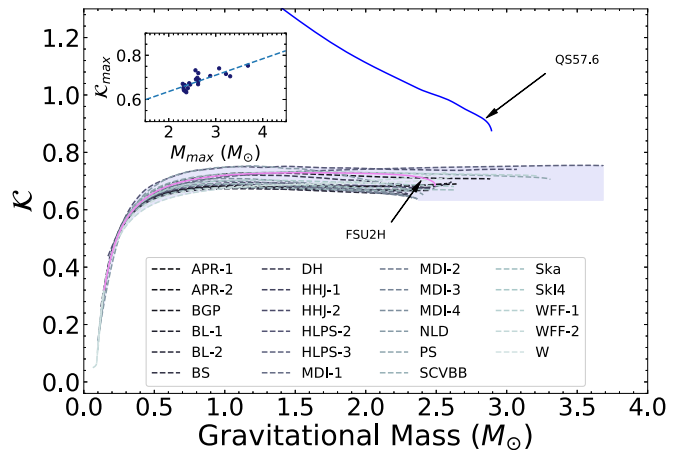


FIG. 9. Kerr parameter dependence on the gravitational mass of a maximally rotating neutron star. Inset: The Kerr parameter values as a function of the corresponding gravitational mass at the maximum mass configuration. The blue dashed line in the inside figure corresponds to the best linear trend. The data at maximum mass configuration for the 23 hadronic EoSs are presented with blue circles in the inside figure. FSU2H and QS57.6 EoSs are also indicated with the two solid lines.

TABLE IV. Coefficients of the empirical relation (28) for the two edges of the window presented in Fig. 9.

Edges	d_1	d_2	d_3
Upper	0.86	-0.12	1.54
Lower	0.86	-0.21	2.67

In addition, in Fig. 9, we plotted the maximum values of the Kerr parameter versus the corresponding gravitational mass. It seems that a linear relation holds between these two quantities, given by the equation

$$\mathcal{K}_{\max} = 0.488 + 0.074 \left(\frac{M_{\max}}{M_{\odot}} \right). \quad (29)$$

There are two important reasons for constraining the Kerr parameter at neutron stars: First, the existence of a maximum value at the Kerr parameter can lead to possible limits for the compactness on neutron stars; strictly speaking, the maximum value of the Kerr parameter for neutron stars implies a maximum value on the possible maximum mass of rotating neutron stars in the universe and, second, can be a criteria for determining the final fate of the collapse of a rotating compact star [49].

Finally, it is clear from Fig. 9 that the Kerr parameter dependence on the gravitational mass of a quark star is quite different than the one on neutron stars. The Kerr parameter of quark stars can be significantly larger than the maximum value of this parameter on neutron stars. In case of the hyperonic EoS, the dependence between gravitational mass and the Kerr parameter exhibits similar behavior with the hadronic ones. A detail study in this direction is in progress.

D. Constant rest mass sequences

The rest mass sequences, also called as time evolutionary sequences, based on an EoS, are roughly horizontal lines that

extend from the Keplerian sequence to the nonrotating end point or at the axisymmetric instability limit [19–21]. The latter depends only on the rest mass value of the selected EoS. For a given EoS, the sequences that are below the rest mass value that corresponds to the maximum mass configuration at the nonrotating model, they have a nonrotating member, and as a consequence, are stable and terminate at the nonrotating model sequence. Above this value, none of the sequences have a nonrotating member. Instead, they are unstable and terminate at the axisymmetric instability limit. The onset that extends from the maximum mass point on the nonrotating limit sequence to the one on the mass-shedding limit sequence is the quasiradial stability limit. The total region that models are unstable is defined via the rest mass sequence that corresponds to the maximum mass configuration of the nonrotating model, as Fig. 10 shows [shadowed (gray) region]. Above this value, the models have masses larger than the maximum mass of the nonrotating model and in that case are called supramassive models [4]. It should be noted that models to the axisymmetric area of the shadowed (gray) region, which is not shown at the corresponding figures, are also unstable.

To be more specific, if a neutron star spin-up by accretion and becomes supramassive, then it would subsequently spin-down along the constant rest mass sequence until it reaches the axisymmetric instability limit and collapse to a black hole. There is a case where some relativistic stars could be born as supramassive ones, or even more, become one as a result of a binary merger. In this case, the star would be initially differentially rotating and collapse would be triggered by a combination between spin-down effect and viscosity (the force that driving the star to uniform rotation) [4].

Although the sequence with rest mass corresponding to the maximum mass configuration of the nonrotating model extends to the right area of the quasiradial stability limit, the unstable one, it is the last one that has a stable part (half

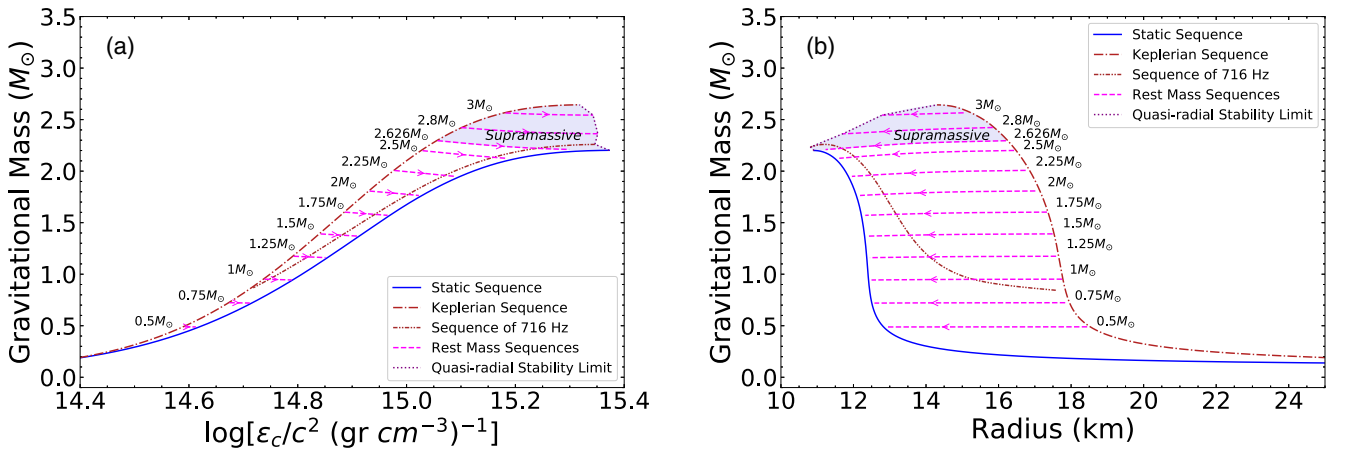


FIG. 10. Normal and supramassive evolutionary sequences of constant rest mass are presented as the dependence of the (a) gravitational mass on the central energy density and (b) gravitational mass on the corresponding radius for the APR-1 EoS. The nonrotating case is presented with the blue solid curve while the maximally rotating one is presented with the red dashed-dotted curve. Constant rest mass sequences are presented with the fuchsia dashed lines, where the rest mass value is also noted. The 716-Hz limit is also presented with the brown dashed-dotted-dotted curve. The quasiradial stability limit is presented with the purple dotted line.

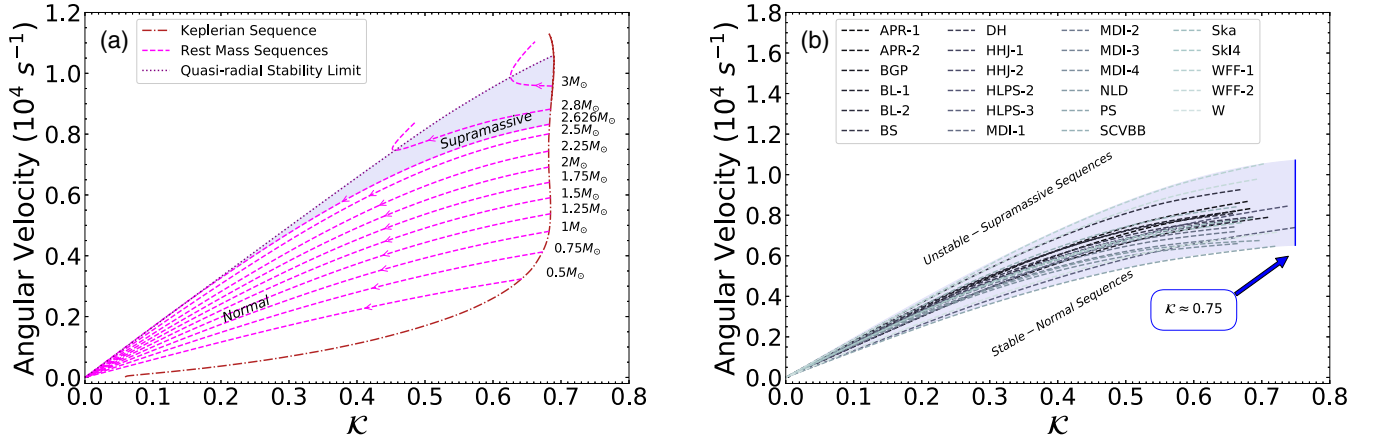


FIG. 11. (a) Normal and supramassive evolutionary sequences of constant rest mass are presented as the dependence of the angular velocity on the Kerr parameter for the APR-1 EoS. Maximally rotating case is presented with the red dashed-dotted curve while the constant rest mass sequences are presented with the fuchsia dashed curves, where the rest mass values are also noted. The quasiradial stability limit is presented with the purple dotted curve. (b) Last stable rest mass sequences for the 23 EoSs as the dependence of angular velocity on the Kerr parameter. Supramassive and normal area are shown to guide the eye. The maximum value of the Kerr parameter is also noted.

of the sequence terminates at the maximum mass configuration of the nonrotating model). While, below this sequence, all the remaining ones are unconditionally stable against gravitational collapse, above this sequence, all sequences would evolve toward catastrophic collapse to a black hole. In Fig. 10, we can see that if we have a neutron star with rest mass in the white region, it would evolve toward stable configuration at the nonrotating sequence, but if we have a star in the shadowed (gray) region, it would subsequently spin-up and evolve toward catastrophic collapse to a black hole [101–103]. The direction of evolution for constant rest mass sequences is noted with the existence of an arrow on them.

In all cases, neutron stars which evolve along normal evolutionary sequences, never spin-up, as they lose angular momentum. In contradiction to neutron stars on normal evolutionary sequences, neutron stars on supramassive ones, because their unstable portion is always at higher angular velocity than the stable portion, at the same value of angular momentum, must spin-up with angular momentum loss in the neighborhood of the stability limit. If the neutron star is massive enough, then the evolutionary sequence (supramassive) exhibit an extended region where spin-up is allowed. This effect may provide us an observable precursor to gravitational collapse to a black hole [49,52]. The latter is shown clearly in Fig. 11(a).

Following the concept from Fig. 11(a), we have constructed the last stable rest mass sequence (LSRMS) for the 23 hadronic EoSs, as shown in Fig. 11(b). This sequence is the one that divides the stable from unstable region, or in other words, the normal from supramassive evolutionary sequences. In Fig. 11(b), we present a window [shadowed (gray) region] where the last stable rest mass sequence can lie and in fact, because the last stable rest mass sequence is the one that corresponds to the maximum mass configuration at the nonrotating model, this is also the region where the EoS can lie, constraining, simultaneously, the spin parameter and

the angular velocity. There is an empirical relation, derived from the data, that can describe this window. The form of this empirical relation is

$$\Omega = (b_1\mathcal{K} + b_2\mathcal{K}^2 + b_3\mathcal{K}^3)10^4 \text{ (s}^{-1}\text{)}, \quad (30)$$

where the coefficients for the two edges are shown in Table V. It is clear from Fig. 11(b) and Eq. (30) that if we have a measurement of angular velocity, or spin parameter, then we could extract the interval where the other parameter can lie.

As a consequence, by constraining simultaneously these two quantities, we could significantly narrow the existing area of EoS.

E. Upper bound for density of cold baryonic matter

Although we employ realistic EoSs to solve numerically equilibrium equations in neutron stars, analytical solutions are far from being insignificant. Useful information can be gained by the comparison between solutions of the Einstein's field equations with numerical solutions for different models of EoSs and the analytical solutions [84]. Two classes derive from analytical solutions: (a) normal neutron stars and (b) self-bound neutron stars. In the first case, the energy density vanishes at the surface where the pressure vanishes and, in the second one, the energy density is finite at the surface.

In this work only the first case scenario will be studied. It is most natural to solve numerically the Tolman-Oppenheimer-Volkoff [(TOV) Einstein's equations for a nonrotating spher-

TABLE V. Coefficients of the empirical relation (30) for the two edges of the window presented in Fig. 11(b).

Edges	b_1	b_2	b_3
Upper	1.94	0.117	-1.058
Lower	1.35	-0.305	-0.449

ical symmetric object] equations [1–3] by introducing an EoS describing the relation between pressure and density which is expected to describe the fluid interior. The other possibility is trying find out analytical solutions of TOV equations with the risk of obtaining solutions without physical interest. Actually, there are hundreds of analytical solutions of TOV equations [104,105]. However, just few of them are of physical interest. Moreover, there are only three that satisfy the criteria that the pressure and energy density vanish on the surface of the star and also that they both decrease monotonically with increasing radius. These three solutions are the Tolman VII, the Buchdahl, and the Nariai IV [106]. The main difference between these analytical solutions is related with the maximum value of compactness at which they took effect. For example, the Buchdahl solution is applicable only for neutron stars with compactness up to the value $\beta = 0.17$ and in general produces soft EoSs. The Tolman VII solution leads to even stiffer EoSs and, consequently, is suitable to describe compact objects with compactness value up to $\beta = 0.34$ (for more details see Ref. [106]). The Nariai IV solution exhibits similar behavior with the Tolman VII. In particular, the Tolman VII is of great interest since it has the specific property that the pressure and density vanish at the surface of the star. It has been extensively employed to neutron star studies and the details of this analytical solution had been given in Appendix C.

It has been shown by Lattimer *et al.* [84] that the Tolman VII solution forms an absolute upper limit, which is confirmed empirically by using a large number of EoSs, in density inside any compact star (see also Refs. [107,108]). This is also the case for rotating stars with rotation rates up to the Keplerian (mass-shedding) rate.

At that time, the maximum masses of the existed EoSs were fully included in the region under the Tolman VII solution; the same holds for the rotating models. In recent years, new EoSs have been introduced and old ones, that could not describe the maximum observed neutron star mass [5–10], have been rejected. In this work, using a total of 23 hadronic EoSs that predict the observed maximum neutron star mass [5–10], we have confirmed that the Tolman VII curve marks the upper limit to the energy density inside a star but without taking into account the rotation (Tolman VII can describe the majority of them). If we add rotation to our models, then this curve is no longer able to describe the new data as they shift, concerning the plotted area, up and left. For this reason, we propose here that if there is a curve, like the Tolman VII solution, shifted to the right, then that would be a suitable solution to fully describe the maximum energy density inside a star. In other words, the existence of this curve can help to form an absolute upper limit in density inside any compact object.

The proposed expression, described by the form

$$\frac{M}{M_{\odot}} = 4.25 \sqrt{\frac{10^{15} \text{ gr cm}^{-3}}{\varepsilon_c/c^2}}, \quad (31)$$

can fully describe both the nonrotating and maximally rotating configuration. The advantages of having this relation are that (a) it can describe the nonrotating configuration having as a

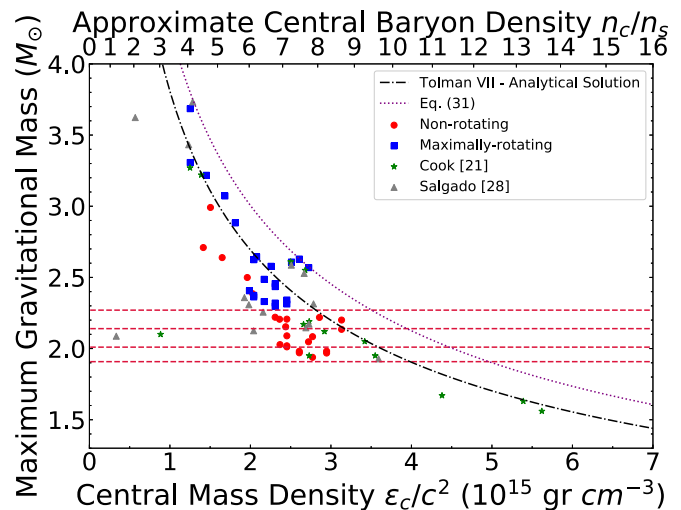


FIG. 12. Gravitational mass dependence on the central energy density and the central baryon density at the maximum mass configuration for the 23 EoSs at the nonrotating and maximally rotating case. Red circles correspond to the nonrotating case, blue squares to the maximally rotating one, green stars to Cook’s [21] data, and gray triangles to Salgado’s [28] data. The red horizontal dashed lines correspond to the observed neutron star mass limits ($1.908M_{\odot}$, $2.01M_{\odot}$, $2.14M_{\odot}$, and $2.27M_{\odot}$). For comparison, the Tolman-VII analytical solution with the black dashed-dotted curve and the Eq. (31) with the purple dotted one are shown.

guide the corresponding maximally rotating one (the Tolman VII analytical solution cannot describe all of them, as displayed in Fig. 12) and (b) it can also describe the maximally rotating configuration.

In Fig. 12 we present the results of the 23 hadronic EoSs, for the nonrotating and maximally rotating case, Cook’s [21] and Salgado’s [28] data, the Tolman VII analytical solution, and the proposed solution (31). The observed neutron star mass limits are also presented to guide the eye.

The knowledge of the central density at the maximally rotating case is important for studying the pulsar’s time evolution. In particular, following the spin-down trail of a millisecond pulsar, the central density increases and the highly compressible quark matter will replace the existed nuclear matter. This effect is directly connected to the reduction of moment of inertia. Henceforth, the central density can inform us on the appearance of a phase transition in its interior. The latter can lead to the important back-bending phenomenon in pulsars [109].

Another interesting effect presented in Fig. 12 is the connection that is established between gravitational mass at the maximum mass configuration and the corresponding central energy density. Besides the fact that it can provide us with the absolute upper limit in density inside any compact star, it can also directly connect the macroscopic properties of neutron star with the microscopic ones.

F. Equation-of-state effects on the braking index of pulsars

It is well known that the angular velocity Ω of an isolated pulsar decreases very slowly with time. Various energy-loss

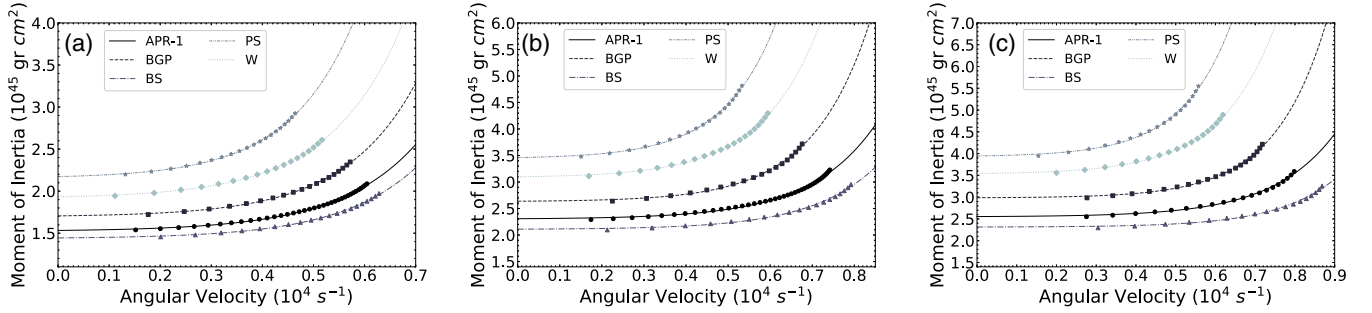


FIG. 13. Constant rest mass sequences as the dependence of moment of inertia on the angular velocity for five representative EoSs and with rest mass corresponding to (a) $M_{\max}^{\text{gr}} = 1.45M_{\odot}$, (b) $M_{\max}^{\text{gr}} = 2M_{\odot}$, and (c) $M_{\max}^{\text{gr}} = 2.2M_{\odot}$. The data and fits for each EoS are presented with the circles and the solid curve for the APR-1, the squares and the dashed curve for the BGP, the triangles and the dashed-dotted curve for the BS, the stars and the dashed-dotted-dotted curve for the PS, and the diamonds and the dotted curve for W.

mechanisms are responsible for this effect, including mainly dipole radiation, charged particles ejections, and gravitational wave radiation [2,110–116]. In this case, and in the most simple model, the evolution of the angular velocity is given by the power law

$$\dot{\Omega} \equiv \frac{d\Omega}{dt} = -\mathcal{J}\Omega^n. \quad (32)$$

The braking index, n , of a pulsar, which describes the dependence of the braking torque on the rotation frequency, is a fundamental parameter of pulsar electrodynamics. Simple theoretical arguments, based on the assumption of a constant dipolar magnetic field, predict $n = 3$. It is easy to show that Eq. (32) leads to the fundamental relation

$$n(\Omega) = \frac{\Omega \ddot{\Omega}}{\dot{\Omega}^2} = 3 - \frac{3\Omega I' + \Omega^2 I''}{2I + \Omega I'}, \quad (33)$$

where a dot corresponds to the derivative with time, $I' = dI/d\Omega$, and $I'' = d^2I/d\Omega^2$. Now, considering the simple power-law dependence $I \sim \Omega^\lambda$, the braking index takes the simple and transparent value

$$n(\Omega) = 3 - \lambda. \quad (34)$$

While for $\lambda = 0$ (moment of inertia independent from angular velocity) we recover the well-known result $n = 3$, in general we expect that the inequality $n(\Omega) \leq 3$ must hold. There is a special case where for some reasons when the denominator of Eq. (33) goes to zero, and then the braking index exhibits a singularity which leads to increasing of Ω with time [2,110,117–120]. This is an interesting effect (which may be caused due to a phase transition in the interior of a pulsar) but we are not going to study it further in this work. Instead, we studied the effects of the EoS on the braking index as well as on the evolution of the angular velocity of a pulsar, especially for very young ones, at their birth, with their angular velocity being at the mass-shedding limit.

In particular, we studied the moment of inertia dependence on the angular velocity for five representative EoSs and for three different values of rest mass. In each case, we produced a fit as shown in Fig. 13, according to the formula

$$I = g_1 + g_2 \exp(g_3 \Omega), \quad (35)$$

where g_1 and g_2 are in units of moment of inertia (10^{45} gr cm^2) and g_3 is in units of time (s).

In order to see how the rest mass effects the braking index, we present in Fig. 14 the five representative EoSs for the different rest masses.

From Fig. 14, it is clear that the rest mass plays an important role on the braking index, i.e., by increasing the rest mass value, the braking index decreases more sharply. This effect will remain valid for all EoSs studied in this paper.

IV. DISCUSSION AND CONCLUSIONS

Different sequences of uniformly rotating neutron stars have been constructed for a large number of hadronic EoSs based on various theoretical nuclear models. In this paper we have studied the bulk properties of neutron stars in correlation with the mass-shedding limit (Keplerian frequency). To be more specific, we have calculated their gravitational and rest mass, equatorial and polar radii, dimensionless angular momentum, angular velocity, moment of inertia, and eccentricity. Relations between the Keplerian frequency and the

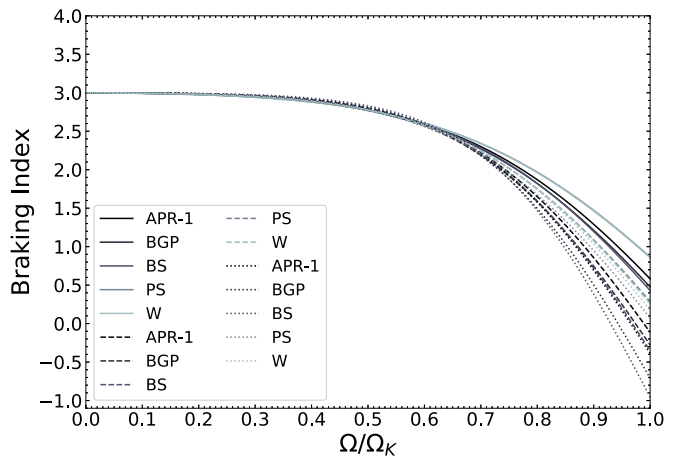


FIG. 14. Braking index dependence on the angular velocity for the five representative EoSs (APR-1, BGP, BS, PS, and W) with constant rest masses. The solid curves correspond to $M_{\max}^{\text{gr}} = 1.45M_{\odot}$, the dashed curves to $M_{\max}^{\text{gr}} = 2M_{\odot}$, and the dotted curves to $M_{\max}^{\text{gr}} = 2.2M_{\odot}$.

bulk properties of neutron stars have been found and shown in the corresponding figures. These universal relations may help to impose constraints on the radius of a neutron star when its mass and Keplerian frequency is well fixed simultaneously. For example, this is the case of a millisecond pulsar (in a binary system) which acquired angular momentum by accretion and becoming a maximally rotating one with measured mass [121].

The dependence of moment of inertia, eccentricity, and Kerr parameter on the total gravitational mass at the Keplerian sequence, is also obtained. In all cases, the EoSs presented similar behavior, so as a follow up, we have studied the dependence of these parameters on the gravitational mass at the maximum mass configuration. We have concluded that moment of inertia and Kerr parameter can provide us with universal relations as a function of the gravitational mass at the maximum mass configuration for the Keplerian frequency. It is also interesting the effect of the eccentricity at the maximum mass configuration for the Keplerian frequency on the corresponding gravitational mass, where it seems that eccentricity behaves as an EoS-independent property. Moreover, we have found that the Kerr parameter reaches a maximum value at around 0.75 (stiffest EoS) for neutron stars. The importance of this result falls under the fact that the gravitational collapse of a uniformly rotating neutron star, constrained to mass-energy and angular momentum conservation, cannot lead to a naked singularity, or in other words, a maximally rotating Kerr black hole [49].

As a limiting case in our study, we presented also an EoS suitable to describe quark stars and one with appearance of hyperons at high densities. In the nonrotating case the results are in good agreement with the hadronic EoSs, whereas in the maximally rotating one, the difference from linearity is obvious. Moreover, as far as concerning the Kerr parameter, it is undeniable that its study on quark stars requires a different approach. Although that a thorough study is needed, we can see that the values of Kerr parameter of quark stars are significantly larger, not only of neutron stars, but also of black holes. The latter can be useful indicator to identify maximally rotating quark stars [49]. However, a detail study must be done in order to acquire the possible effects of the EoS on quark stars and their similarities with neutron stars. Concerning the hyperonic EoS, while its consistent with our 23 hadronic EoSs allows it to be studied with them, a detailed study mainly based on hyperonic EoSs would be more suitable.

Normal and supramassive sequences of constant rest mass for a specific EoS have been constructed. In the corresponding figures, we present the stability and instability region of a neutron star. This is possible by plotting the evolution of a neutron star along the constant rest mass sequences. The extraordinary effect of supramassive ones is that they can inform us about the gravitational collapse to a black hole. The gravitational collapse of a rotating neutron star to a black hole creates a black hole with almost the same mass and angular momentum as the initial star (small amount of total mass and angular momentum carried away by gravitation radiation [122]) and therefore the same Kerr parameter. Henceforth, this effect may provide us an observable precursor to gravitational col-

lapse to a black hole. It is important to add here that this effect will remain valid for all the EoSs studied in this paper.

In order to imply possible constraints on the EoS, we have constructed the LSRMS for the variety of the EoSs and the dimensionless moment of inertia. In particular, we have presented them in a figure of the angular velocity as a function of the Kerr parameter and the dimensionless moment of inertia as a function of the compactness parameter, respectively. In both cases, we have extracted a window where these properties can lie. In the first case, concerning the LSRMS, because this sequence is the one that corresponds to the maximum mass configuration at the nonrotating model, this is also the window where the EoS can lie, constraining, simultaneously, the angular velocity and spin parameter (or Kerr parameter) on neutron stars. In the second case, the window that is formed can help us to constrain moment of inertia and compactness parameter. The latter can impose strong constraints in radius of neutron stars, which is one of the open problems in nuclear astrophysics.

Afterward, we have updated the work of Lattimer and Prakash [84] by using EoSs which are consistent with the current observed limits of neutron star mass [5–10]. In this work we propose the possible existence of an empirical solution, similarly to the Tolman VII analytical solution, for neutron stars, using as a guide the maximally rotating configuration in order to describe both the nonrotating and the maximally rotating configurations. The existence of this solution can help to define the ultimate density of cold baryonic matter by setting an absolute upper limit at the central energy density. The latter can be a useful insight because it can inform about the appearance of a phase transition in the interior of the star and its leading to the back-bending phenomenon in pulsars.

Finally, we have studied the effects of the EoSs on the braking index of pulsars. Braking index, as an intrinsic property of neutron star's structure, can inform us about the rate of change of angular velocity. Although we know it is very slow, after 70% of the Keplerian angular velocity, the braking index is undergoing significant changes through the influence of the rest mass. This specific area, from 70% to 100% of the Keplerian angular velocity, may provide us with useful insights on the constitution of the dense nuclear matter.

In the near future, neutron stars mergers and measurements of gravitational waves, besides the fact that are a powerful tool to study compact objects, such as neutron stars and black holes, will be able to provide us with the Keplerian frequency of these objects. In fact, the remnant formed in the immediate aftermath of the GW170817 merger, although believed to have been differentially rotating and not uniformly, contains sufficient angular momentum to be near its mass-shedding limit [123]. The observational measurement of Keplerian frequency, along with the theoretical predictions, would provide us with strong constraints on the high-density part of the EoS.

ACKNOWLEDGMENTS

The authors thank Prof. N. Stergioulas for providing the RNS code [91] and his very useful comments and clari-

fications. Ch.C.M thanks the Theoretical Astrophysics Department of the University of Tuebingen, where part of this work was performed, and Prof. K. Kokkotas for his useful comments on the preparation of the manuscript. We also thank Dr. T. Athanasiadis for his useful correspondence. Furthermore, we thank the anonymous referees for their valuable comments and suggestions which helped us to improve the present paper. This work was partially supported by the COST

action PHAROS (CA16214) and the DAAD Germany-Greece Grant No. ID 57340132.

APPENDIX A: THE MDI MODEL

In order to study specific properties and evolutionary process of neutron stars we employed the MDI model. The energy per particle, according to MDI, is given by [64,88]

$$\begin{aligned}
 E_b(n, I) = & \frac{3}{10} E_F^0 u^{2/3} [(1+I)^{5/3} + (1-I)^{5/3}] + \frac{1}{3} A \left[\frac{3}{2} - X_0 I^2 \right] u + \frac{\frac{2}{3} B \left[\frac{3}{2} - X_3 I^2 \right] u^\sigma}{1 + \frac{2}{3} B' \left[\frac{3}{2} - X_3 I^2 \right] u^{\sigma-1}} \\
 & + \frac{3}{2} \sum_{i=1,2} \left[C_i + \frac{C_i - 8Z_i}{5} I \right] \left(\frac{\Lambda_i}{k_F^0} \right)^3 \left\{ \frac{[(1+I)u]^{1/3}}{\frac{\Lambda_i}{k_F^0}} - \tan^{-1} \frac{[(1+I)u]^{1/3}}{\frac{\Lambda_i}{k_F^0}} \right\} \\
 & + \frac{3}{2} \sum_{i=1,2} \left[C_i - \frac{C_i - 8Z_i}{5} I \right] \left(\frac{\Lambda_i}{k_F^0} \right)^3 \left\{ \frac{[(1-I)u]^{1/3}}{\frac{\Lambda_i}{k_F^0}} - \tan^{-1} \frac{[(1-I)u]^{1/3}}{\frac{\Lambda_i}{k_F^0}} \right\}, \quad (A1)
 \end{aligned}$$

where $I = (n_n - n_p)/n$, $X_0 = x_0 + 1/2$, and $X_3 = x_3 + 1/2$.

In Eq. (A1), the ratio u is defined as $u = n/n_s$, with n_s denoting the equilibrium symmetric nuclear matter density (or saturation density) and equals 0.16 fm^{-3} . The parameters A , B , σ , C_1 , C_2 , and B' , which are called coupling constants and appear in the description of symmetric nuclear matter (SNM), are determined so that the relation $E_b(n_s, 0) = -16 \text{ MeV}$ holds. The finite-range parameters are $\Lambda_1 = 1.5k_F^0$ and $\Lambda_2 = 3k_F^0$ with k_F^0 being the Fermi momentum at the saturation density n_s . By suitably choosing the rest parameters x_0 , x_3 , Z_1 , and Z_2 , which appear in the description for asymmetric nuclear matter, it is possible to obtain different forms for the density dependence of symmetry energy as well as the value of slope parameter L and the value of symmetry energy at the saturation density [64,88]. Actually, for each value of L , the density dependence of symmetry energy is adjusted so that the energy of pure neutron matter is comparable with those of the existing *state-of-the-art* calculations [64,88].

APPENDIX B: OBSERVED FREQUENCY LIMIT

Lattimer and Prakash derived a relation in Ref. [90], which gives the Keplerian frequency of a rotating neutron star, in terms of radius R and mass M of the corresponding nonrotating neutron star. The relation is

$$f_k = 1045 \left(\frac{M}{M_\odot} \right)^{1/2} \left(\frac{10 \text{ km}}{R} \right)^{3/2} \text{ (Hz)}, \quad (B1)$$

which can be written as $f_k \approx 0.5701 f_s$, where f_s is the Keplerian rate for a rigid Newtonian sphere is given by the equation

$$f_s = 1833 \left(\frac{M}{M_\odot} \right)^{1/2} \left(\frac{10 \text{ km}}{R} \right)^{3/2} \text{ (Hz)}. \quad (B2)$$

Following the work of Riahi *et al.* [58], in order to find a more accurate relation, we have constructed a relation, based on a three order polynomial fit in terms of mass and radius of

the corresponding nonrotating neutron star, given by the form

$$\begin{aligned}
 f_k/f_s = & 0.559 + 2.69 \left(\frac{M}{M_\odot} \right) \left(\frac{\text{km}}{R} \right) \\
 & - 20.28 \left[\left(\frac{M}{M_\odot} \right) \left(\frac{\text{km}}{R} \right) \right]^2 + 55.74 \left[\left(\frac{M}{M_\odot} \right) \left(\frac{\text{km}}{R} \right) \right]^3, \quad (B3)
 \end{aligned}$$

with error up to 4%, in comparison with Lattimer and Prakash where the error was up to 30%.

For the observed frequency of the fastest known pulsar, PSR J1748-2446ad, which rotates with a frequency of 716 Hz, we obtained the relation (B3) and its schematic presentation is presented in Fig. 2.

APPENDIX C: TOLMAN VII ANALYTICAL SOLUTION

The basic ingredients of the Tolman VII analytical solution of Einstein's equations for a nonrotating spherical symmetric object, which in this case is neutron star, are presented below.

The metric functions are defined as follows:

$$e^{-\lambda} = 1 - \beta x^2 (5 - 3x^2), \quad e^\nu = \left(1 - \frac{5\beta}{3} \right) \cos^2 \phi, \quad (C1)$$

where

$$x = \frac{r}{R}, \quad \phi = \frac{w_1 - w}{2} + \phi_1, \quad \phi_1 = \tan^{-1} \sqrt{\frac{\beta}{3(1-2\beta)}}$$

and

$$w = \ln \left(x^2 - \frac{5}{6} + \sqrt{\frac{e^{-\lambda}}{3\beta}} \right), \quad w_1 = \ln \left(\frac{1}{6} + \sqrt{\frac{1-2\beta}{3\beta}} \right).$$

The energy density and the pressure read as

$$\frac{\mathcal{E}(x)}{\mathcal{E}_c} = (1 - x^2), \quad \mathcal{E}_c = \frac{15Mc^2}{8\pi R^3}, \quad (C2)$$

$$\frac{P(x)}{\mathcal{E}_c} = \frac{2}{15} \sqrt{\frac{3e^{-\lambda}}{\beta}} \tan \phi - \frac{1}{3} + \frac{x^2}{5}. \quad (C3)$$

There are some constraints related with the validity of the Tolman VII analytical solution. In particular, the central value of pressure becomes infinite for $\beta = 0.3862$, while the speed of sound remains less than the speed of light only for $\beta < 0.2698$ [106]. This solution leads to a stable configurations only for $\beta < 0.3428$ [106].

-
- [1] S. L. Shapiro and S. A. Teukolsky, *Black Holes, White Dwarfs, and Neutron Stars* (John Wiley & Sons, New York, 1983).
- [2] N. K. Glendenning, *Compact Stars: Nuclear Physics, Particle Physics, and General Relativity* (Springer, Berlin, 2000).
- [3] P. Haensel, A. Y. Potekhin, and D. G. Yakovlev, *Neutron Stars I: Equation of State and Structure* (Springer-Verlag, New York, 2007).
- [4] J. L. Friedman and N. Stergioulas, *Rotating Relativistic Stars* (Cambridge University Press, Cambridge, 2013).
- [5] P. Demorest, T. Pennucci, S. Ransom, M. Roberts, and J. Hessels, *Nature* **467**, 1081 (2010).
- [6] E. Fonseca, T. T. Pennucci *et al.*, *Astrophys. J.* **832**, 167 (2016).
- [7] Z. Arzoumanian, *Astrophys. J. Suppl. Ser.* **235**, 37 (2018).
- [8] J. Antoniadis, P. C. Freire, N. Wex, T. M. Tauris, R. S. Lynch *et al.*, *Science* **340**, 1233232 (2013).
- [9] H. T. Cromartie, E. Fonseca, S. M. Ransom *et al.*, *Nat. Astron.* **4**, 72 (2020).
- [10] M. Linares, T. Shahbaz, and J. Casares, *Astrophys. J.* **859**, 54 (2018).
- [11] A. Patruno, B. Haskell, and N. Andersson, *Astrophys. J.* **850**, 106 (2017).
- [12] J. W. T. Hessels, S. M. Ransom, I. H. Stairs, P. C. C. Freire, V. M. Kaspi, and F. Camile, *Science* **311**, 1901 (2006).
- [13] M. P. Prakash, *J. Phys.* **84**, 927 (2015).
- [14] M. Bejger, T. Bulik, and P. Haensel, *Mon. Not. Roy. Astron. Soc.* **364**, 635 (2005).
- [15] N. Stergioulas, *Liv. Rev. Relat.* **1**, 8 (1998).
- [16] V. Paschalidis and N. Stergioulas, *Liv. Rev. Relat.* **20**, 7 (2017).
- [17] S. L. Shapiro, S. A. Teukolsky, and I. Wasserman, *Nature* **340**, 451 (1989).
- [18] G. B. Cook, S. L. Shapiro, and S. A. Teukolsky, *Astrophys. J.* **398**, 203 (1992).
- [19] G. B. Cook, S. L. Shapiro, and S. A. Teukolsky, *Astrophys. J.* **422**, 227 (1994).
- [20] G. B. Cook, S. L. Shapiro, and S. A. Teukolsky, *Astrophys. J. Lett.* **423**, L117 (1994).
- [21] G. B. Cook, S. L. Shapiro, and S. A. Teukolsky, *Astrophys. J.* **424**, 823 (1994).
- [22] J. L. Friedman, J. R. Ipser, and L. Parker, *Astrophys. J.* **304**, 115 (1986).
- [23] J. L. Friedman and J. R. Ipser, *Astrophys. J.* **314**, 594 (1987).
- [24] J. L. Friedman, J. R. Ipser, and R. D. Sorkin, *Astrophys. J.* **325**, 722 (1988).
- [25] J. L. Friedman, J. R. Ipser, and L. Parker, *Phys. Rev. Lett.* **62**, 3015 (1989).
- [26] S. Koranda, N. Stergioulas, and J. L. Friedman, *Astrophys. J. Lett.* **488**, 799 (1997).
- [27] P. Haensel and J. L. Zdunik, *Nature* **340**, 617 (1989).
- [28] M. Salgado, S. Bonazzola, E. Gourgoulhon, and P. Haensel, *Astron. Astrophys. Supl.* **108**, 455 (1994).
- [29] M. Salgado, S. Bonazzola, E. Gourgoulhon, and P. Haensel, *Astron. Astrophys.* **291**, 155 (1994).
- [30] P. Haensel, M. Salgado, and S. Bonazzola, *Astron. Astrophys.* **296**, 745 (1995).
- [31] J. P. Lasota, P. Haensel, and M. A. Abramowicz, *Astrophys. J.* **456**, 300 (1996).
- [32] P. Haensel, J. P. Lasota, and J. L. Zdunik, *Astron. Astrophys.* **344**, 151 (1999).
- [33] F. Weber and N. K. Glendenning, *Phys. Lett. B* **265**, 1 (1991).
- [34] F. Weber and N. K. Glendenning, *Astrophys. J.* **390**, 541 (1992).
- [35] N. K. Glendenning, *Phys. Rev. D* **46**, 4161 (1992).
- [36] N. K. Glendenning and F. Weber, *Phys. Rev. D* **50**, 3836 (1994).
- [37] M. A. Abramowicz and R. V. Wagover, *Astrophys. J.* **226**, 1063 (1978).
- [38] L. Lindblom, *Astrophys. J.* **303**, 146 (1986).
- [39] J. M. Lattimer, M. Prakash, D. Masak, and A. Yahil, *Astrophys. J.* **355**, 241 (1990).
- [40] M. Hashimoto, K. Oyamatsu, and Y. Eriguchi, *Astrophys. J.* **436**, 257 (1994).
- [41] K. Iida and K. Sato, *Astrophys. J.* **477**, 294 (1997).
- [42] M. Shibata, T. W. Baumgarte, and S. L. Shapiro, *Phys. Rev. D* **61**, 044012 (2000).
- [43] O. Benhar, V. Ferrari, L. Gualtieri, and S. Marassi, *Phys. Rev. D* **72**, 044028 (2005).
- [44] S. K. Dhiman, R. Kumar, and B. K. Agrawal, *Phys. Rev. C* **76**, 045801 (2007).
- [45] P. G. Krastev, B. A. Li, and A. Worley, *Astrophys. J.* **676**, 1170 (2008).
- [46] B. K. Agrawal, R. Kumar, and S. K. Dhiman, *Phys. Rev. D* **77**, 087301 (2008).
- [47] P. Haensel, J. L. Zdunik, and M. Bejger, *New. Astr. Rev.* **51**, 785 (2008).
- [48] P. Haensel, J. L. Zdunik, M. Bejger, and J. M. Lattimer, *Astron. Astrophys.* **502**, 605 (2009).
- [49] K. W. Lo and L. M. Lin, *Astrophys. J.* **728**, 12 (2011).
- [50] N. B. Zhang, B. Qi, S. Y. Wang, S. L. Ge, and B. Y. Sun, *Int. J. Mod. Phys. E* **22**, 1350085 (2013).
- [51] S. Chakrabarti, T. Delsate, N. Grlebeck, and J. Steinhoff, *Phys. Rev. Lett.* **112**, 201102 (2014).
- [52] F. Cipolletta, C. Cherubini, S. Filippi, J. A. Rueda, and R. Ruffini, *Phys. Rev. D* **92**, 023007 (2015).
- [53] C. Breu and L. Rezzolla, *Mon. Not. Roy. Astron. Soc.* **459**, 646 (2016).
- [54] P. Haensel, M. Bejger, M. Fortin, and L. Zdunik, *Eur. Phys. J.* **52**, 59 (2016).
- [55] M. Bejger, D. Blaschke, P. Haensel, J. L. Zdunik, and M. Fortin, *Astron. Astrophys.* **600**, A39 (2017).
- [56] F. Cipolletta, C. Cherubini, S. Filippi, J. A. Rueda, and R. Ruffini, *Phys. Rev. D* **96**, 024046 (2017).

- [57] B. Haskell, J. L. Zdunik, M. Fortin, M. Bejger, R. Wijnands, and A. Patruno, *Astron. Astrophys.* **620**, A69 (2018).
- [58] R. Riahi, S. Z. Kalantari, and J. A. Rueda, *Phys. Rev. D* **99**, 043004 (2019).
- [59] M. Marques, M. Oertel, M. Hempel, and J. Novak, *Phys. Rev. C* **96**, 045806 (2017).
- [60] N. D. Batra, K. P. Nunna, and S. Banik, *Phys. Rev. C* **98**, 035801 (2018).
- [61] D. D. Doneva, S. S. Yazadjiev, N. Stergioulas, and K. D. Kokkotas, *Phys. Rev. D* **88**, 084060 (2013).
- [62] S. S. Yazadjiev, D. D. Doneva, and K. D. Kokkotas, *Phys. Rev. D* **91**, 084018 (2015).
- [63] P. S. Koliogiannis and C. C. Moustakidis, *Astroph. Space Sci.* **364**, 52 (2019).
- [64] M. Prakash, I. Bombaci, Manju Prakash, P. J. Ellis, J. M. Lattimer, and R. Knorren, *Phys. Rep.* **280**, 1 (1997).
- [65] Ch. C. Moustakidis and C. P. Panos, *Phys. Rev. C* **79**, 045806 (2009).
- [66] H. Heiselberg and M. Hjorth-Jensen, *Phys. Rep.* **328**, 237 (2000).
- [67] E. Chabanat, P. Bonche, P. Haensel, J. Meyer, and R. Schaeffer, *Nucl. Phys. A* **627**, 710 (1997).
- [68] M. Farine, J. M. Pearson, and F. Tondeur, *Nucl. Phys. A* **615**, 135 (1997).
- [69] F. Douchin and P. Haensel, *Astron. Astrophys.* **380**, 151 (2001).
- [70] T. Gaitanos and M. Kaskulov, *Nucl. Phys. A* **899**, 133 (2013).
- [71] T. Gaitanos and M. Kaskulov, *Nucl. Phys. A* **940**, 181 (2015).
- [72] J. D. Walecka, *Ann. Phys.* **83**, 491 (1974).
- [73] K. Hebeler, J. M. Lattimer, C. J. Pethick, and A. Schwenk, *Astrophys. J.* **773**, 11 (2013).
- [74] B. K. Sharma, M. Centelles, X. Vinas, M. Baldo, and G. F. Burgio, *Astron. Astrophys.* **584**, A103 (2015).
- [75] S. Balberg and S. L. Shapiro, [arXiv:astro-ph/0004317](https://arxiv.org/abs/astro-ph/0004317).
- [76] R. L. Bowers, A. M. Gleeson, and R. D. Pedigo, *Phys. Rev. D* **12**, 3056 (1975).
- [77] I. Bombaci and D. Logoteta, *Astron. Astrophys.* **609**, A128 (2018).
- [78] R. B. Wiringa, V. Fiks, and A. Fabrocini, *Phys. Rev. C* **38**, 1010 (1988).
- [79] V. R. Pandharipande and R. A. Smit, *Phys. Lett. B* **59**, 15 (1975).
- [80] A. Akmal, V. R. Pandharipande, and D. G. Ravenhall, *Phys. Rev. C* **58**, 1804 (1998).
- [81] R. Feynman, N. Metropolis, and E. Teller, *Phys. Rev.* **75**, 1561 (1949).
- [82] G. Baym, C. Pethik, and P. Sutherland, *Astrophys. J.* **170**, 299 (1971).
- [83] L. Tolos, M. Centelles, and A. Ramos, *Pub. Astron. Soc. Aust.* **34**, E065 (2017).
- [84] J. M. Lattimer and M. Prakash, *Phys. Rev. Lett.* **94**, 111101 (2005).
- [85] K. Hebeler and A. Schwenk, *Phys. Rev. C* **82**, 014314 (2010).
- [86] C. Constantinou, B. Muccioli, M. Prakash, and J. M. Lattimer, *Phys. Rev. C* **89**, 065802 (2014).
- [87] C. Constantinou, B. Muccioli, M. Prakash, and J. M. Lattimer, *Phys. Rev. C* **92**, 025801 (2015).
- [88] Ch. C. Moustakidis, *Phys. Rev. C* **91**, 035804 (2015).
- [89] Ch. C. Moustakidis, *Phys. Rev. C* **78**, 054323 (2008).
- [90] J. M. Lattimer and M. Prakash, *Science* **304**, 536 (2004).
- [91] <https://www.gravity.phys.uwm.edu/rms/>
- [92] N. Stergioulas and J. L. Friedman, *Astrophys. J.* **444**, 306 (1995).
- [93] H. Komatsu, Y. Eriguchi, and I. Hachisu, *Mon. Not. Roy. Astron. Soc.* **237**, 355 (1989).
- [94] N. Stergioulas, *Liv. Rev. Relat.* **6**, 3 (2003).
- [95] J. M. Lattimer and B. F. Schutz, *Astrophys. J.* **629**, 979 (2005).
- [96] K. S. Virbhadra and G. F. R. Ellis, *Phys. Rev. D* **62**, 084003 (2000).
- [97] K. S. Virbhadra and G. F. R. Ellis, *Phys. Rev. D* **65**, 103004 (2002).
- [98] K. S. Virbhadra and C. R. Keeton, *Phys. Rev. D* **77**, 124014 (2008).
- [99] K. S. Virbhadra, *Phys. Rev. D* **79**, 083004 (2009).
- [100] K. S. Thorne, *Astrophys. J.* **191**, 507 (1974).
- [101] M. Shibata, *Astrophys. J.* **595**, 992 (2003).
- [102] P. D. Lasky, B. Haskell, V. Ravi, E. J. Howell, and D. M. Coward, *Phys. Rev. D* **89**, 047302 (2014).
- [103] V. Ravi and P. D. Lasky, *Mon. Not. R. Astron. Soc.* **441**, 2433 (2014).
- [104] D. Kramer, H. Stephani, M. A. MacCallum, and E. Hertl, *Exact Solutions of Einstein's Field Equations* (Deutsche Verlag der Wissenschaften, Berlin/Cambridge University Press, Cambridge, 1980).
- [105] M. S. R. Delgaty and K. Lake, *Comput. Phys. Commun.* **115**, 395 (1998).
- [106] Ch. C. Moustakidis, *Gen. Relativ. Gravit.* **49**, 68 (2017).
- [107] J. M. Lattimer and M. Prakash, *Quarks, Nuclei and Stars: Memorial Volume Dedicated to Gerald E. Brown* (World Scientific, Singapore, 2011), p. 275.
- [108] N. B. Zhang and B. A. Li, *Eur. Phys. J. A* **55**, 39 (2019).
- [109] N. K. Glendenning, *Nucl. Phys. A* **638**, 239c (1998).
- [110] F. Weber, *Pulsars as Astrophysical Laboratories for Nuclear and Particle Physics* (Taylor & Francis, London, 1999).
- [111] D. Lorimer and M. Kramer, *Handbook of Pulsar Astronomy* (Cambridge University Press, Cambridge, 2005).
- [112] O. Hamil, J. R. Stone, M. Urbanec, and G. Urbancova, *Phys. Rev. D* **91**, 063007 (2015).
- [113] *Neutron Stars and Pulsars* (Astrophysics and Space Science Library Vol. 357), edited by W. Becker (Springer, Berlin, 2009).
- [114] A. G. Lyne, C. A. Jordan, F. Graham-Smith, C. M. Espinoza, B. W. Stappers, and P. Weltevrede, *Mon. Not. Roy. Astron. Soc.* **446**, 857 (2015).
- [115] D. R. Lorimer, *Liv. Rev. Relat.* **11**, 8 (2008).
- [116] R. N. Manchester, G. B. Hobbs, A. Teoh, and M. Hobbs, *Astron. J.* **129**, 1993 (2005).
- [117] N. K. Glendenning, S. Pei, and F. Weber, *Phys. Rev. Lett.* **79**, 1603 (1997).
- [118] H. Heiselberg and M. Hjorth-Jensen, *Phys. Rev. Lett.* **80**, 5485 (1998).
- [119] J. L. Zdunik, M. Bejger, P. Haensel, and E.ourgoulhon, *Astron. Astrophys.* **450**, 747 (2006).
- [120] P. Bagchi, A. Das, B. Layek, and A. M. Srivastava, *Phys. Lett. B* **747**, 120 (2015).
- [121] J. M. Lattimer, *JPS Conf. Proc.* **14**, 010801 (2017).
- [122] L. Baiotti, I. Hawke, L. Rezzolla, and E. Schnetter, *Phys. Rev. Lett.* **94**, 131101 (2005).
- [123] J. M. Lattimer, *Universe* **5**, 159 (2019).